Response of surface shortwave cloud radiative effect to greenhouse gases and aerosols and its impact on summer maximum temperature

Tao Tang[1], Drew Shindell[1], Yuqiang Zhang[1], Apostolos Voulgarakis[2], Jean-Francois Lamarque[3], Gunnar Myhre[4], Camilla W. Stjern[4], Gregory Faluvegi[5, 6], Bjørn H. Samset[4]

[1]Division of Earth and Ocean Sciences, Duke University, Durham, NC, USA
[2]Department of Physics, Imperial College London, London, UK
[3]National Center for Atmospheric Research, Boulder, CO, USA
[4]CICERO, Center for International Climate and Environment Research, Oslo, Norway
[5]Center for Climate System Research, Columbia University, New York, NY, USA
[6]NASA Goddard Institute for Space Studies, New York, NY, USA

Correspondence to: Tao Tang (tao.tang@duke.edu)

Abstract. Shortwave cloud radiative effects (SWCRE), defined as the difference of shortwave radiative flux between all-sky and clear-sky conditions at the surface, have been reported to play an important role in influencing the Earth's energy budget and temperature extremes. In this study, we employed a set of global climate models to examine the SWCRE responses to CO_2, black carbon (BC) aerosols and sulfate aerosols in boreal summer over the Northern Hemisphere. We found that CO_2 causes positive SWCRE changes over most of the NH, and BC causes similar positive responses over North America, Europe and East China but negative SWCRE over India and tropical Africa. When normalized by effective radiative forcing, the SWCRE from BC is roughly 3-5 times larger than that from CO_2. SWCRE change is mainly due to cloud cover changes resulting from the changes in relative humidity (RH) and, to a lesser extent, changes in cloud liquid water, circulation, dynamics and stability. The SWCRE response to sulfate aerosols, however, is negligible compared to that for CO_2 and BC because part of the radiation scattered by clouds under all-sky conditions will also be scattered by aerosols under clear-sky conditions. Using a multilinear regression model, it is found that mean daily maximum temperature (Tmax) increases by 0.15 K and 0.13 K per W m^{-2} increase in local SWCRE under the CO_2 and BC experiment, respectively. When domain-averaged, the contribution of SWCRE change to summer mean Tmax changes was 10-30% under CO_2 forcing and 30-50% under BC forcing, varying by regions, which can have important implications for extreme climatic events and socio-economic activities.

1 Introduction

Clouds have a pivotal role in influencing the Earth's energy budget (Ramanathan et al., 1989). By enhancing the planetary albedo, clouds exert a global mean shortwave cloud radiative effects (SWCRE) of about -50 W m^{-2} at the top-of-the-atmosphere, and by contributing to the greenhouse effect, exert a mean longwave effect (LWCRE) of approximately +30 W m^{-2} (Boucher et al., 2013). On the whole, clouds cause a net forcing of -20 W m^{-2} relative to a cloud-free Earth, which is approximately five times as large as the radiative forcing from a doubling of CO_2 concentration. Therefore, a subtle change in cloud properties has the potential to cause significant impacts on climate (Boucher et al., 2013; Zelinka et al., 2017). Recent studies contended that the cloud feedback, especially the shortwave (SW) cloud feedback, is very likely to be positive (Clement et al., 2009; Dessler, 2010; Zelinka et al., 2017). As the SW cloud feedback is positively correlated with the net climate feedback parameter (Andrews et al., 2012; Andrews et al., 2015; Zhou et al., 2016), a stronger positive SW cloud feedback will lead to higher climate sensitivity and may lead to a future warming towards the high end of current projections (Zhai et al., 2015; Andrews et al., 2018).

On seasonal scales, SWCRE is strongest in the summer months when the solar heating is strongest (Harrison et al., 1990). Because SWCRE is in effect only during daytime, it can substantially modify daily maximum temperature (Tmax). For instance, Dai et al. (1999) found that increased cloud cover can reduce Tmax, thereby decreasing diurnal temperature range. Tang and Leng (2012) reported that the damped Tmax over Eurasia could be partially explained by the cloud cover increase during 1982-2009. As a positive feedback, SWCRE at the surface has also been reported to play a role in heatwave and drought

events over Europe by enhancing solar heating (Rowell & Jones, 2006; Vautard et al., 2007; Zampieri et al., 2009; Chiriaco et al., 2014; Myers et al., 2018). This has influenced the environment, ecosystems and the economy through affecting the frequency and intensity of forest fires, power cuts, transport restrictions, crop failure and loss of life (De Bono et al., 2004;

60   Ciais et al., 2005; Robine et al., 2008). For example, Wetherald and Manabe (1995) reported that in the summer for mid-latitude continents, higher temperature enhances evaporation in the spring and then evaporation decreases in the summer due to depleted soil moisture. Combined with higher temperature, this summertime evaporation reduction leads to lower relative humidity (RH), which reduces cloud cover and thereby invigorates solar heating. Cheruy et al. (2014) revealed that the inter-model spread of summer temperature projections in Northern mid-latitudes in CMIP5 (Climate Model Inter-comparison

65   Project Phase 5) models is greatly influenced by SWCRE.

All the above studies suggest that the SWCRE plays an important role in influencing the surface energy budget and extreme temperature. Well-mixed greenhouse gases (WMGHGs) and aerosols are currently the two largest anthropogenic forcings (Myhre et al., 2013b). A better understanding on the climate response to these individual forcing agents is increasingly needed,

70   considering their different trends across the globe and opposite impacts on climate (Shindell & Faluvegi, 2009). Due to the difficulty of separating the forced climate signal of a single agent within observational records, these studies are generally based on model simulations, such as the widely used quadrupling of CO_2 experiments (Andrews et al., 2012). Many attempts have also been made to explore the aerosol impact on clouds and Earth's energy balance (Lohmann & Feichter, 2005; Chung & Soden, 2017), mean temperature (Ruckstuhl et al., 2008; Philipona et al., 2009), as well as extreme temperature (Sillmann

75   et al., 2013; Xu et al., 2018). However, all these studies treated aerosols as a whole and the individual impacts from absorbing and scattering aerosols are still less understood. Though some studies investigated the impact from individual aerosol species (Williams et al., 2001; Chuang et al., 2002; Koch & Del Genio, 2010), they generally used only a single model, and the results may be subject to model biases (Flato et al., 2013). Moreover, due to the continuing increase in the likelihood of hot temperature extremes (Seneviratne et al., 2014), as well as their serious consequences (De Bono et al., 2004), it is imperative

80   to have a better understanding on the role of SWCRE from individual forcing agents in hot extremes. However, a multi-model study on the cloud response to individual aerosol species and the impact of that response on Tmax is still lacking. Given these knowledge gaps, here we investigate the changes of SWCRE to CO_2, BC and sulfate aerosols individually and explore its potential impact on Tmax by using a set of state-of-the-art global climate models. CO_2 is the most dominant WMGHG while the latter two represent absorbing and scattering aerosols respectively. This paper will proceed as follows: data and methods

85   are described in Section 2. Results are presented in Section 3, discussions and summary are given in Section 4.

2 Data and Methods

2.1 Data

This study employs the model output from groups participating in the Precipitation Driver and Response Model Intercomparison Project (PDRMIP), utilizing simulations examining the climate responses to individual climate drivers (Myhre et al., 2017). The nine models used in this study are CanESM2, GISS-E2R, HadGEM2, HadGEM3, MIROC, CESM-CAM4, CESM-CAM5, NorESM and IPSL-CM5A. The versions of most models used in the PDRMIP are essentially the same as their CMIP5 versions. The configurations and basic settings are listed in Table 1. In these simulations, global-scale perturbations were applied to all the models: a doubling of CO_2 concentration ($CO_2\times2$), a tenfold increase of present-day black carbon concentration/emission ($BC\times10$), and a fivefold increase of present-day SO_4 concentration/emission ($SO_4\times5$). All perturbations were abrupt. Each perturbation was run in two parallel configurations, a 15-year fixed sea surface temperature (fsst) simulation and a 100-year coupled simulation. One model (CESM-CAM4) used a slab ocean setup for the coupled simulation whereas the others used a full dynamic ocean. CO_2 was applied relative to the models' baseline values. For aerosol perturbations, monthly year 2000 concentrations were derived from the AeroCom Phase II initiative (Myhre et al., 2013a) and multiplied by the stated factors in concentration-driven models. Some models were unable to perform simulations with prescribed concentrations. These models multiplied emissions by these factors instead (Table 1). The aerosol loadings in the CanESM2 model for the two aerosol perturbations are shown in Fig. 1 for illustrative purpose; the spatial patterns are similar for other models. In the BC experiment, the concentration is highest in East China (E. China), followed by India and tropical Africa. For the SO_4 simulations, the aerosols are mainly restricted to the Northern Hemisphere (NH), with the highest loading observed in E. China, followed by India and Europe. The eastern US also has moderately high concentrations. It is noted that only three of the nine models include aerosol-cloud interactions while the remaining ones only have aerosol-radiation interactions. However, this does not impact our main conclusions (see section 4). More detailed descriptions of PDRMIP and its initial findings are given in Samset et al. (2016), Myhre et al. (2017), Liu et al. (2018) and Tang et al. (2018).

2.2 Methods

In this study, we focus on the SWCRE at the surface in the low and mid-latitudes during boreal summer months (June-July-August, JJA hereafter), which is calculated as the difference in the SW radiative flux at the surface between all-sky and clear-sky conditions (Ramanathan et al., 1989). The base state of SWCRE in each model is shown in Fig. S1, with a multi-model mean (MMM) value of -57.9 ± 1.8 W m^{-2} (MMM±1 standard error). The spatial patterns are fairly consistent across the models, with strong SWCRE in tropical regions and mid-to-high latitudes and weaker SWCRE in subtropics, regions generally with less clouds. Changes in SWCRE are obtained by subtracting the control simulations from the perturbations using the data of the last 20 years in each coupled simulation. The changes are then normalized by the effective radiative forcing (ERF) in the corresponding experiments to obtain the changes per unit global forcing for comparison. Previous studies demonstrated that climate changes linearly with climate forcing for various forcing agents, including BC (Hansen et al., 2005; Mahajan et al.,

2013). The ERF values for each model are obtained from Tang et al. (2019), which diagnosed those from the data for years 6-15 of the fsst simulations of each perturbation by calculating the radiative flux changes at the top-of-the-atmosphere (Hansen et al., 2002). The MMM ERF values are 3.65 ± 0.09 W m^{-2} ($CO_2\times2$), 1.16 ± 0.25 W m^{-2} ($BC\times10$), and -3.52 ± 0.63 W m^{-2} ($SO_4\times5$) for indicated experiments, respectively (MMM±1 standard error). Then the MMM changes are estimated by averaging all the nine models' results, giving the same weighting factor to each model. A two-sided student t-test is used to examine whether the MMM results are significantly different from zero. The same process was also repeated to other variables analyzed (i.e., temperature and humidity).

In order to investigate the impact of circulation changes on specific humidity, following Banacos and Schultz (2005), the horizontal moisture flux convergence (MFC) is calculated as:

$$MFC = -\nabla \cdot (qV) = -V \cdot \nabla q - q\nabla \cdot V \qquad (1)$$

In Eq (1), q is specific humidity in g kg^{-1}, and V is horizontal wind including both zonal and meridional components. All variables have a monthly temporal resolution. Equation (1) could be further written as:

$$MFC = -u\frac{\partial q}{\partial x} - v\frac{\partial q}{\partial y} - q(\frac{\partial u}{\partial x} + \frac{\partial v}{\partial y}) \qquad (2)$$

In which u and v are zonal and meridional wind components in m s^{-1}.

3 Results

3.1 SWCRE Change

Figure 2a-c show the SWCRE changes in response to abrupt changes in CO_2, BC and SO_4. CO_2 causes positive changes in SWCRE over most areas in the NH, indicating that more SW radiation reaches the surface. BC causes similar changes, but with enhanced (ERF-normalized) magnitude, especially in North America (N. America), Europe and East Asia (E. Asia). In some source regions of BC aerosols (tropical Africa and India), however, the SWCRE changes are negative, which means more SW was reflected. These changes are all statistically significant and are unlikely to be caused by natural variability. When it comes to individual model response (Fig. S2-S3), these patterns are also consistent across at least eight of the nine models and are not very sensitive to the model setup (emission-based or concentration-based). For SO_4, the SWCRE changes are relatively small compared with the other two forcings and few significant changes are found over low-to-mid latitude regions. When domain averaged (green boxes in Fig. 2), the MMM SWCRE from CO_2 forcing is, 1.7 W m^{-2} (N. America), 2.0 W m^{-2} (Europe) and 1.5 W m^{-2} (E. China) respectively for the indicated regions. The SWCRE of BC forcing is 7.0 W m^{-2} (N.

America), 9.0 W m^{-2} (Europe) and 9.4 W m^{-2} (E. China) respectively, which is roughly 3 to 5 times larger than that from CO_2

150   forcing whereas sulfate aerosols induced 1.2 W m^{-2} over E. China and near-zero impact in N. America and Europe, with even the sign of change being uncertain (Fig. 3 and Fig. S4). Such SWCRE changes could be largely explained by the changes of cloud cover (Fig. 2d-f). Low-level cloud cover decreased significantly in regions where SWCRE is positive for CO_2 and BC forcing, with a stronger decrease from the latter, indicating that the cloud response is more sensitive to BC forcing than to WMGHGs. The sulfate aerosols caused increased cloud cover over mid-latitudes (Fig. 2f). The cloud cover in other levels

155   show similar patterns of change (Fig. S5). In order to better understand these cloud responses, we will explore a set of potential mechanisms driving such changes.

3.2 Mechanism of the Cloud Changes

Clouds form when air rises and cools to saturation, and are thus closely linked to changes in RH (Fig. 4a-c). The general pattern of RH changes corresponds well with cloud cover changes (Fig. 2d-f). That is, the cloud cover decreases in regions where the

160   RH drops and vice versa for most areas. A larger RH reduction due to BC compared with CO_2 also aligns with a larger cloud cover decrease under BC forcing, especially over N. America and Europe. This spatial pattern is not surprising as it is easier for air masses to reach saturation in conditions with higher RH. By definition, RH depends on both specific humidity and saturation vapor pressure (which, in turn, depends on temperature). To probe which factor determines the RH changes, we further analyzed specific humidity changes (Fig. 4d-f). Specific humidity increases ubiquitously under both CO_2 and BC

165   scenarios, as a result of increased evaporation in a warmer climate. Thus, the main driver of the RH drop is the atmospheric temperature that drives a faster increase of saturation vapor pressure. Figure 5 shows the changes of vapor pressure as a function of temperature change over Europe at 850 hPa. For example, the temperature increases by ~1.1 K under CO_2 forcing, accompanied by ~0.02 kPa vapor pressure increase. Such a vapor pressure increase, however, cannot keep pace with the rise in saturation vapor pressure, which is about 0.1 kPa. Consequently, the RH decreases in Europe and this is also the case for

170   most other land areas. BC causes stronger temperature increases (and hence larger RH drop) in Europe and N. America, explaining the larger cloud cover reductions compared with CO_2. In the source regions of BC, such as India and tropical Africa, the RH increases because of stronger increases of specific humidity, combined with weak or no temperature changes (Fig. S6). The response of cloud liquid water in the BC experiment could further support this conclusion (Fig. 4h). Liquid water decreases (increases) in regions with decreasing (increasing) cloud cover, following the pattern of RH. As cloud water content directly

175   impacts cloud optical thickness and albedo, such a response may further impact SWCRE (i.e., enhance reflectance in regions showing increasing liquid water and enhance transmittance in regions with decreasing liquid water). However, the liquid water responses under CO_2 and sulfate aerosols are much weaker, only significant in part of Asia and tropical Africa (Fig. 4g and i).

Changes in moisture flux, dynamics and stability may also play a role in altering specific humidity and cloud formation

180   (Bretherton, 2015). Here we analyze the changes of MFC, vertical velocity (omega), as well as lower tropospheric stability (LTS), and find significant changes under the BC experiment again (Fig. 6). It is seen that more moisture is transported to

tropical Africa and India (Fig. 6b), which could explain the abovementioned increases of specific humidity in these regions despite their lack of warming. A similar response was noted by Liu et al. (2018), which suggested that more moisture could be brought into monsoon regions due to BC forcing. Koch and Del Genio (2010) noted that BC particles could promote cloud cover in convergent regions as they enhance deep convection and low-level convergence when drawing in moisture from ocean to land regions. This is also observed in our analyses, for example over Africa, North India, Pakistan and part of North China (Fig. 6b and e), which is consistent with the dynamic cloud response mechanism noted by Myers and Norris (2013). However, these impacts may be further compounded by cloud type, circulation and the altitude of BC particles relative to the clouds (Koch & Del Genio, 2010; Samset & Myhre, 2015). The changes in moisture flux and dynamics in the CO_2 experiment are relatively weaker compared with those from BC, and most of the changes are only observed in low-latitude regions, possibly due to the shift of Intertropical Convergence Zone (ITCZ) or monsoon circulations. The sulfate aerosols, on the other hand, generally show opposite changes to those from CO_2 and BC (Fig. 4c and f), owing to sulfate's cooling effect. Another mechanism that has been reported to influence cloud cover is LTS, in which a stable boundary layer could trap more moisture, thereby permitting more low-level clouds (Wood & Bretherton, 2006; Bretherton, 2015). In order to investigate this mechanism, we further analyzed LTS, defined as the difference of potential temperature between 700 hPa and surface (Fig. 6g-i), in which positive anomalies indicate a stronger inversion or weaker lapse rate. The LTS response is again strongest in response to BC forcing (Fig. 6h), with a widespread increase in stability. A previously reported positive correlation between LTS and low-level cloud cover is, nonetheless, only observed in BC source regions (tropical Africa and India) and part of the central US (Fig. 6h). The LTS responses over land are much weaker in response to CO_2 and SO_4 forcing, with some responses in Africa and India in response to sulfate aerosols (weaker inversion and less cloud). Some other factors have also been suggested to play a role in modifying low-level clouds, such as the diurnal cycle (Caldwell & Bretherton, 2009) and radiative effects of cirrus clouds (Christensen et al., 2013). Due to the limited model output, however, we acknowledge that it is impossible to examine these factors in the current study and it is beyond the scope of our study to probe all possible factors driving the cloud changes. In summary, the above analyses illustrate that the cloud cover changes we see can be primarily explained by RH changes and, to a lesser extent, changes of liquid water content, circulation, dynamics, and stability.

3.3 Fast and Slow Responses

The above responses shown are total responses, which could be further split into fast responses (also called rapid adjustments) and slow responses (Andrews et al., 2010; Boucher et al., 2013). The fast responses generally occur within weeks to a few months with the global mean temperature unchanged, and also with the expectation of a small change over land, which could be obtained by fsst simulations. The slow response is mainly depending on global mean temperature change, which could be estimated by the difference between coupled simulations and fsst simulations, assuming the total response is a linear combination of fast response and slow response (Samset et al., 2016; Stjern et al., 2017). For the CO_2 experiment, fast responses dominated in E. US and Europe while both fast and slow responses influence Asia (Fig. 7). When it comes to BC, both fast and slow responses are important in these regions, and in some regions the fast and slow response even show opposite changes

215 (e.g., N. Europe). This is consistent with the findings of Stjern et al. (2017) that the response of cloud amount under BC forcing typically consists of opposite rapid adjustments. Regarding sulfate aerosols, the SWCRE changes are much weaker, with both fast and slow responses influencing Asia and Africa. As discussed in Section 3.2, the slow responses in Asia is likely to be associated with circulation changes, as significant changes in MFC, omega and stability are observed in tropical regions and monsoon regions across all three experiments (Fig. 6). These circulation changes could be, but are not limited to, shifts in the

220 monsoons or ITCZ and tropical expansion, and both greenhouse gases and aerosols have been reported to impact these circulations (Menon et al., 2002; Wang, 2007; Meehl et al., 2008; Seidel et al., 2008; Allen et al., 2012; Turner & Annamalai, 2012).

3.4 SWCRE Response to Sulfate Aerosol

Another interesting phenomenon worth noting is the relatively small change in SWCRE induced by sulfate aerosols compared

225 with CO_2 and BC. SWCRE at the surface is obtained as the difference of SW fluxes between all-sky and clear-sky conditions (Fig. 8). However, both clouds and aerosol particles scatter solar radiation, so that at least part of the radiation scattered by clouds under all-sky conditions will also be scattered by aerosols under clear-sky conditions (no clouds). This means the SW radiation change at the surface due to scattering may not be as sensitive to cloud fraction changes, which leads to reduced changes in their difference (SWCRE), at least in the source regions (Fig. 8). The SWCRE under sulfate aerosols will not be

230 further discussed due to its small radiative impact at the surface.

3.5 Impact on Radiation and Tmax

From the energy perspective, the net incoming radiation (Rin) at the surface is the combination of downward SW radiation and downward longwave (LW) radiation minus the reflected SW radiation (Rin = ↓SW − ↑SW + ↓LW). Rin represents the total energy available to maintain the surface temperature and to sustain the turbulent fluxes (Philipona et al., 2009). The

235 surface responds to the imposed Rin by redistributing the altered energy content among the outgoing LW radiation and nonradiative fluxes (ground heat flux and turbulent flux) (Wild et al., 2004). Because SW radiation is in effect only during daytime while LW radiation works both day and night, Rin is directly related to Tmax. In a perturbed climate, both SW and LW radiation will change, thereby changing Rin and Tmax. The net SW radiation change is further linearly decomposed into SW changes under clear-sky conditions and SWCRE changes. The changes of Rin and its individual components, as well as

240 Tmax are shown in Fig. 9. For the $CO_2 \times 2$ experiment, the SW under clear-sky conditions shows slight decreases over most of land surfaces, mainly due to the absorption of SW radiation by enhanced water vapor, except for some high-latitude regions where albedo effect is important (Fig. 9a). Combined with the changes of SWCRE and ↓LW radiation, Rin shows significant increases over all land surfaces and thus, increasing Tmax (Fig. 9g and i). The BC×10 experiment shows similar responses, with significantly negative SW radiation under clear-sky conditions due to SW absorption by BC particles (Fig. 9b) and

245 enhanced ↓LW radiation resulted from atmospheric heating (Fig. 9f). The resulting Rin changes largely explained Tmax changes on the first order, with cooling observed in source regions (India and tropical Africa) and warming elsewhere (Fig. 9h

and j). Nonetheless, some exceptions occurred (i.e., E. China), with decreased Rin but increased Tmax, possibly due to the atmospheric heat transport (Menon et al., 2002) and reduced turbulent fluxes (Wild et al., 2004).

250 In order to further determine the contributions in Tmax changes from each individual radiative component, a multilinear regression model is applied by regressing Tmax changes to SW clear-sky, SWCRE and ↓LW radiation changes with zero intercept, obtaining the following models:

$CO_2 \times 2$:
255 $Tmax = 0.08 \times SW_{clear-sky} + 0.15 \times SWCRE + 0.14 \times \downarrow LW$ ($R^2 = 0.73$, $p < 0.001$)

$BC \times 10$:
$Tmax = 0.05 \times SW_{clear-sky} + 0.13 \times SWCRE + 0.15 \times \downarrow LW$ ($R^2 = 0.80$, $p < 0.001$)

260 All values in the linear models are MMM changes in each experiment. The models could explain 73% and 80% of the Tmax change in $CO_2 \times 2$ and $BC \times 10$ experiment respectively. The coefficients represent the Tmax change under unit radiative flux change, in which the Tmax increases by 0.15 K (0.13 K) per unit increase in local SWCRE under the CO_2 (BC) experiment respectively. Furthermore, the coefficients demonstrate that Tmax changes are more sensitive to unit SWCRE and ↓LW changes than to unit $SW_{clear-sky}$. A comparison of the original Tmax values and the fitted values from the linear models is shown
265 in Figure 10. The linear models predict the Tmax changes fairly well, with the values scattering along the one-to-one line. The contributions from each radiative component to Tmax changes were estimated with the linear models and the domain-averaged changes for N. America, Europe, E. China and India (purple boxes in Fig. 9a) are listed in Table 2. Physically, Tmax increases in these regions are mainly due to the increased flux from SWCRE and ↓LW, and partially offset by the reduced flux from $SW_{clear-sky}$ (Table 2 & Fig. 9). Taking N. America under $CO_2 \times 2$ experiment as an example, the warming in Tmax from SWCRE
270 and ↓LW are 0.95 K and 3.24 K respectively, in which SWCRE contributed roughly by 23% to the total warming and the remaining 77% is from the ↓LW radiation change. Such warming is offset by the 0.27 K cooling from SW changes under clear-sky conditions, leading to a net increase of 3.92 K in Tmax. The contributions of SWCRE in Tmax increases are 29% (Europe), 20% (E. China) and 9% (India) for the indicated regions under the $CO_2 \times 2$ experiment. For the $BC \times 10$ experiment, the contributions from SWCRE are larger than those in the CO_2 experiment, i.e. 34% (N. America), 47% (Europe) and 34%
275 (E. China) for each region. The response over India under the BC experiment is opposite, in which both SW components cause cooling in Tmax due to reduced fluxes and such cooling is slightly offset by the warming from increased ↓LW radiation. In this case, the negative SWCRE change contributed 54% to the reduction in Tmax. It is noted that the radiation change might not explain all Tmax changes, as other factors may come into play. For instance, the temperature response would be different when surface is getting drier under a warmer climate. This is because more net radiation is realized as sensible heat instead of

280 latent heat under drier conditions, which has been suggested to play an important role in recent European heatwaves (Seneviratne et al., 2006; Fischer et al., 2007).

4 Discussion and Summary

Our study shows that cloud cover in the summer is reduced in a warming climate over most mid-latitude land regions. The reduction of clouds, at the same time, may also reduce the warming effect by reducing downwelling LW radiation (LWCRE,

285 Fig. S7). Specifically, the LWCRE changes per unit CO_2 forcing, in MMM, are -1.1 W m^{-2} (N. America), -0.8 W m^{-2} (Europe) and -1.0 W m^{-2} (E. China) respectively, resulting in net CRE (SWCRE+LWCRE) changes of 0.6 W m^{-2} (N. America), 1.2 W m^{-2} (Europe) and 0.5 W m^{-2} (E. China) at the surface. The LWCRE changes per unit BC forcing are -1.7 W m^{-2} (N. America), -2.1 W m^{-2} (Europe) and -1.5 W m^{-2} (E. China) respectively, leading to net CRE changes of 5.3 W m^{-2} (N. America), 6.9 W m^{-2} (Europe) and 7.9 W m^{-2} (E. China). The net CRE changes are positive under both forcings and work as a positive feedback

290 in these areas. As SWCRE is only active during daytime, the CRE changes have an even more pronounced amplifying effect on summer extreme temperature in these populated regions.

Recent European heatwave events have been linked to the shift of mean temperature (Schär et al., 2004; Barriopedro et al., 2011). Thus, the enhanced increase in summer mean Tmax may significantly increase the number of hot days and the

295 probability of heatwave events. Our model simulations show that both N. America and Europe show faster increases in Tmax than in Tmin (daily minimum temperature) under both CO_2 and BC experiments (figure not shown), indicating an increase in diurnal temperature range, which has also been reported by Wang and Dillon (2014). These changes can have substantial socio-economic impacts (De Bono et al., 2004; Ciais et al., 2005), influencing human health (Robine et al., 2008), labor productivity (Kjellstrom et al., 2018), and disease transmission (Paaijmans et al., 2010), as well as environmental and other ecological

300 functions (Vasseur David et al., 2014; Wang & Dillon, 2014).

Some limitations also exist in the current study. Firstly, aerosol-cloud interactions cannot be realistically represented, as more than half of the PDRMIP simulations were run with fixed concentrations, where changes in cloud lifetime cannot affect aerosols. For the BC simulations, three models include aerosol indirect effects (MIROC, NorESM and IPSL) while the

305 remaining ones have only aerosol-radiation interactions included (instantaneous and rapid adjustments). The responses of SWCRE for the two categories are shown in Figure 11. For the regions of interest in the current study, the positive SWCRE over N. America, Europe and E. China and negative SWCRE over India are still observed in the models including indirect effects, but with reduced magnitude. Thus, our main conclusions hold in both sets of models, since the responses do not qualitatively vary between those with indirect effects and models without those effects. Such effects are not likely to be a large

310 source of uncertainty but merit future study. Secondly, the aerosol perturbations are idealized time-invariant 10× and 5× present-day aerosol concentrations. Such simulations provide valuable physical insights into the effects of different forcings

on a variety of aspects of the climate system. Aerosol concentrations, however, changed inhomogeneously during the historical period and in recent decades, both spatially and temporally. For example, aerosol concentrations have been decreasing in Europe and N. America since the 1980s and have been increasing in Asia since the 1950s (Smith et al., 2011). Future simulations may use aerosol forcing with realistic spatio-temporal changes.

In conclusion, our study shows that both CO_2 and BC could cause positive SWCRE changes over most regions in the NH, with a stronger response caused by BC, except over some key source regions of BC aerosols (e.g., India, tropical Africa) which show opposite changes. The SWCRE changes under sulfate aerosol forcing are, however, relatively small compared with the other two forcers. The SWCRE changes are mainly a consequence of RH changes and, to a lesser extent, liquid water, circulation, dynamics and stability changes. The SWCRE changes may have contributed 10~50% of summer mean Tmax increases, depending on forcing agent and region, and contributed substantially to Tmax decreases in the source regions of India and Africa, which has important implications for extreme climatic events and socio-economic activities.

Data code availability

The PDRMIP model output used in this study are available to public through the Norwegian FEIDE data storage facility. For more information, please see http://cicero.uio.no/en/PDRMIP. This study is performed by using Matlab R 2019a. The Matlab code is available upon reasonable request.

Competing interests

The authors declare no competing interests.

Author contributions

T.T. and D.S. designed this study. T.T. performed data analysis and wrote the initial manuscript. All authors contributed to scientific discussion, results framing and manuscript polishing.

Acknowledgement

We thank the two reviewers for their helpful and constructive comments. We acknowledge the NASA High-End Computing Program through the NASA Center for Climate Simulation at Goddard Space Flight Center for computational resources to run the GISS-E2R model and support from NASA GISS. PDRMIP is partly funded through the Norwegian Research Council project NAPEX (project number 229778). A.Voulgarakis is supported by NERC under grant NE/K500872/1. Computing

resources for CESM1-CAM5 (ark:/85065/d7wd3xhc) simulations were provided by the Climate Simulation Laboratory at NCAR Computational and Information System Laboratory, sponsored by the National Science Foundation and other agencies.

340

References

Allen, R. J., Sherwood, S. C., Norris, J. R., & Zender, C. S. (2012). Recent northern hemisphere tropical expansion primarily driven by black carbon and tropospheric ozone. *Nature, 485*(7398), 350-354. doi:10.1038/nature11097

Andrews, T., Forster, P. M., Boucher, O., Bellouin, N., & Jones, A. (2010). Precipitation, radiative forcing and global temperature change. *Geophysical Research Letters, 37*. doi:10.1029/2010gl043991

Andrews, T., Gregory, J. M., Paynter, D., Silvers, L. G., Zhou, C., Mauritsen, T., et al. (2018). Accounting for changing temperature patterns increases historical estimates of climate sensitivity. *Geophysical Research Letters, 45*(16), 8490-8499. doi:10.1029/2018gl078887

Andrews, T., Gregory, J. M., & Webb, M. J. (2015). The dependence of radiative forcing and feedback on evolving patterns of surface temperature change in climate models. *Journal of Climate, 28*(4), 1630-1648. doi:10.1175/Jcli-D-14-00545.1

Andrews, T., Gregory, J. M., Webb, M. J., & Taylor, K. E. (2012). Forcing, feedbacks and climate sensitivity in cmip5 coupled atmosphere-ocean climate models. *Geophysical Research Letters, 39*. doi:10.1029/2012gl051607

Arora, V., Scinocca, J., Boer, G., Christian, J., Denman, K., Flato, G., et al. (2011). Carbon emission limits required to satisfy future representative concentration pathways of greenhouse gases. *Geophysical Research Letters, 38*(5). doi:10.1029/2010GL046270

Banacos, P. C., & Schultz, D. M. (2005). The use of moisture flux convergence in forecasting convective initiation: Historical and operational perspectives. *Weather and Forecasting, 20*(3), 351-366. doi:10.1175/WAF858.1

Barriopedro, D., Fischer, E. M., Luterbacher, J., Trigo, R. M., & García-Herrera, R. (2011). The hot summer of 2010: Redrawing the temperature record map of europe. *Science, 332*(6026), 220. doi:10.1126/science.1201224

Bellouin, N., Rae, J., Jones, A., Johnson, C., Haywood, J., & Boucher, O. (2011). Aerosol forcing in the climate model intercomparison project (cmip5) simulations by hadgem2-es and the role of ammonium nitrate. *Journal of Geophysical Research: Atmospheres, 116*(D20). doi:10.1029/2011JD016074

Bentsen, M., Bethke, I., Debernard, J., Iversen, T., Kirkevåg, A., Seland, Ø., et al. (2013). The norwegian earth system model, noresm1-m—part 1: Description and basic evaluation of the physical climate. *Geosci. Model Dev, 6*(3), 687-720. doi:10.5194/gmd-6-687-2013

Boucher, O., Randall, D., Artaxo, P., Bretherton, C., Feingold, G., Forster, P., et al. (2013). Clouds and aerosols. In *Climate change 2013: The physical science basis. Contribution of working group i to the fifth assessment report of the intergovernmental panel on climate change* (pp. 571-657). Cambridge, UK and New York, USA: Cambridge University Press.

Bretherton, C. S. (2015). Insights into low-latitude cloud feedbacks from high-resolution models. *Philosophical Transactions of the Royal Society A: Mathematical, Physical and Engineering Sciences, 373*(2054), 20140415. doi:10.1098/rsta.2014.0415

Caldwell, P., & Bretherton, C. S. (2009). Large eddy simulation of the diurnal cycle in southeast pacific stratocumulus. *Journal of the Atmospheric Sciences, 66*(2), 432-449. doi:10.1175/2008JAS2785.1

Cheruy, F., Dufresne, J. L., Hourdin, F., & Ducharne, A. (2014). Role of clouds and land-atmosphere coupling in midlatitude continental summer warm biases and climate change amplification in cmip5 simulations. *Geophysical Research Letters, 41*(18), 6493-6500. doi:10.1002/2014GL061145

Chiriaco, M., Bastin, S., Yiou, P., Haeffelin, M., Dupont, J.-C., & Stéfanon, M. (2014). European heatwave in july 2006: Observations and modeling showing how local processes amplify conducive large-scale conditions. *Geophysical Research Letters, 41*(15), 5644-5652. doi:10.1002/2014GL060205

Christensen, M. W., Carrió, G. G., Stephens, G. L., & Cotton, W. R. (2013). Radiative impacts of free-tropospheric clouds on the properties of marine stratocumulus. *Journal of the Atmospheric Sciences, 70*(10), 3102-3118. doi:10.1175/JAS-D-12-0287.1

Chuang, C. C., Penner, J. E., Prospero, J. M., Grant, K. E., Rau, G. H., & Kawamoto, K. (2002). Cloud susceptibility and the first aerosol indirect forcing: Sensitivity to black carbon and aerosol concentrations. *Journal of Geophysical Research: Atmospheres, 107*(D21), AAC 10-11-AAC 10-23. doi:10.1029/2000JD000215

Chung, E.-S., & Soden, B. J. (2017). Hemispheric climate shifts driven by anthropogenic aerosol–cloud interactions. *Nature Geoscience, 10*, 566. doi:10.1038/ngeo2988

Ciais, P., Reichstein, M., Viovy, N., Granier, A., Ogée, J., Allard, V., et al. (2005). Europe-wide reduction in primary productivity caused by the heat and drought in 2003. *Nature, 437*(7058), 529-533. doi:10.1038/nature03972

Clement, A. C., Burgman, R., & Norris, J. R. (2009). Observational and model evidence for positive low-level cloud feedback. *Science, 325*(5939), 460. doi:10.1126/science.1171255

Collins, W., Bellouin, N., Doutriaux-Boucher, M., Gedney, N., Halloran, P., Hinton, T., et al. (2011). Development and evaluation of an earth-system model–hadgem2. *Geoscientific Model Development, 4*(4), 1051-1075. doi:10.5194/gmd-4-1051-2011

390   Dai, A., Trenberth, K. E., & Karl, T. R. (1999). Effects of clouds, soil moisture, precipitation, and water vapor on diurnal temperature range. *Journal of Climate, 12*(8), 2451-2473. doi:10.1175/1520-0442(1999)012<2451:EOCSMP>2.0.CO;2

De Bono, A., Peduzzi, P., Kluser, S., & Giuliani, G. (2004). *Impacts of summer 2003 heat wave in europe*. Retrieved from https://www.unisdr.org/files/1145_ewheatwave.en.pdf

Dessler, A. E. (2010). A determination of the cloud feedback from climate variations over the past decade. *Science, 330*(6010), 1523-1527. doi:10.1126/science.1192546

395   Dufresne, J.-L., Foujols, M.-A., Denvil, S., Caubel, A., Marti, O., Aumont, O., et al. (2013). Climate change projections using the ipsl-cm5 earth system model: From cmip3 to cmip5. *Climate Dynamics, 40*(9-10), 2123-2165. doi:10.1007/s00382-012-1636-1

Fischer, E. M., Seneviratne, S. I., Vidale, P. L., Lüthi, D., & Schär, C. (2007). Soil moisture–atmosphere interactions during the 2003 european summer heat wave. *Journal of Climate, 20*(20), 5081-5099. doi:10.1175/JCLI4288.1

Flato, G., Marotzke, J., Abiodun, B., Braconnot, P., Chou, S.-C., Collins, W., et al. (2013). Evaluation of climate models. In *Climate change*
400   *2013 – the physical science basis: Working group i contribution to the fifth assessment report of the intergovernmental panel on climate change* (pp. 741-866). Cambridge, UK and New York, USA: Cambridge University Press.

Gent, P. R., Danabasoglu, G., Donner, L. J., Holland, M. M., Hunke, E. C., Jayne, S. R., et al. (2011). The community climate system model version 4. *Journal of Climate, 24*(19), 4973-4991. doi:10.1175/2011JCLI4083.1

Hansen, J., Sato, M., Nazarenko, L., Ruedy, R., Lacis, A., Koch, D., et al. (2002). Climate forcings in goddard institute for space studies
405   si2000 simulations. *Journal of Geophysical Research: Atmospheres, 107*(D18). doi:10.1029/2001JD001143

Hansen, J., Sato, M., Ruedy, R., Nazarenko, L., Lacis, A., Schmidt, G. A., et al. (2005). Efficacy of climate forcings. *Journal of Geophysical Research-Atmospheres, 110*(D18). doi:doi:10.1029/2005JD005776

Harrison, E. F., Minnis, P., Barkstrom, B. R., Ramanathan, V., Cess, R. D., & Gibson, G. G. (1990). Seasonal-variation of cloud radiative forcing derived from the earth radiation budget experiment. *Journal of Geophysical Research-Atmospheres, 95*(D11), 18687-
410   18703. doi:DOI 10.1029/JD095iD11p18687

Hurrell, J. W., Holland, M. M., Gent, P. R., Ghan, S., Kay, J. E., Kushner, P. J., et al. (2013). The community earth system model: A framework for collaborative research. *Bulletin of the American Meteorological Society, 94*(9), 1339-1360. doi:10.1175/BAMS-D-12-00121.1

Iversen, T., Bentsen, M., Bethke, I., Debernard, J., Kirkevåg, A., Seland, Ø., et al. (2013). The norwegian earth system model, noresm1-m-
415   part 2: Climate response and scenario projections. *Geoscientific Model Development, 6*(2), 389. doi:10.5194/gmd-6-389-2013

Kay, J., Deser, C., Phillips, A., Mai, A., Hannay, C., Strand, G., et al. (2015). The community earth system model (cesm) large ensemble project: A community resource for studying climate change in the presence of internal climate variability. *Bulletin of the American Meteorological Society, 96*(8), 1333-1349. doi:10.1175/BAMS-D-13-00255.1

Kirkevåg, A., Iversen, T., Seland, Ø., Hoose, C., Kristjánsson, J., Struthers, H., et al. (2013). Aerosol–climate interactions in the norwegian
420   earth system model–noresm1-m. *Geoscientific Model Development, 6*(1), 207-244. doi:10.5194/gmd-6-207-2013

Kjellstrom, T., Freyberg, C., Lemke, B., Otto, M., & Briggs, D. (2018). Estimating population heat exposure and impacts on working people in conjunction with climate change. *International Journal of Biometeorology, 62*(3), 291-306. doi:10.1007/s00484-017-1407-0

Koch, D., & Del Genio, A. D. (2010). Black carbon semi-direct effects on cloud cover: Review and synthesis. *Atmos. Chem. Phys., 10*(16), 7685-7696. doi:10.5194/acp-10-7685-2010

425   Liu, L., Shawki, D., Voulgarakis, A., Kasoar, M., Samset, B. H., Myhre, G., et al. (2018). A pdrmip multimodel study on the impacts of regional aerosol forcings on global and regional precipitation. *Journal of Climate, 31*(11), 4429-4447. doi:10.1175/jcli-d-17-0439.1

Lohmann, U., & Feichter, J. (2005). Global indirect aerosol effects: A review. *Atmospheric Chemistry and Physics, 5*, 715-737. doi:DOI 10.5194/acp-5-715-2005

430   Mahajan, S., Evans, K. J., Hack, J. J., & Truesdale, J. E. (2013). Linearity of climate response to increases in black carbon aerosols. *Journal of Climate, 26*(20), 8223-8237. doi:10.1175/JCLI-D-12-00715.1

Meehl, G. A., Arblaster, J. M., & Collins, W. D. (2008). Effects of black carbon aerosols on the indian monsoon. *Journal of Climate, 21*(12), 2869-2882. doi:10.1175/2007jcli1777.1

Menon, S., Hansen, J., Nazarenko, L., & Luo, Y. (2002). Climate effects of black carbon aerosols in china and india. *Science, 297*(5590),
435   2250-2253. doi:10.1126/science.1075159

Myers, T. A., Mechoso, C. R., Cesana, G. V., DeFlorio, M. J., & Waliser, D. E. (2018). Cloud feedback key to marine heatwave off baja california. *Geophysical Research Letters, 45*(9), 4345-4352. doi:10.1029/2018GL078242

Myers, T. A., & Norris, J. R. (2013). Observational evidence that enhanced subsidence reduces subtropical marine boundary layer cloudiness. *Journal of Climate, 26*(19), 7507-7524. doi:10.1175/JCLI-D-12-00736.1

440   Myhre, G., Forster, P., Samset, B., Hodnebrog, Ø., Sillmann, J., Aalbergsjø, S., et al. (2017). Pdrmip: A precipitation driver and response model intercomparison project, protocol and preliminary results. *Bulletin of the American Meteorological Society*(2016). doi:10.1175/BAMS-D-16-0019.1

Myhre, G., Samset, B., Schulz, M., Balkanski, Y., Bauer, S., Berntsen, T., et al. (2013a). Radiative forcing of the direct aerosol effect from aerocom phase ii simulations. *Atmospheric Chemistry and Physics, 13*(4), 1853. doi:10.5194/acp-13-1853-2013

445 Myhre, G., Shindell, D., Bréon, F.-M., Collins, W., Fuglestvedt, J., Huang, J., et al. (2013b). Anthropogenic and natural radiative forcing. In T. F. Stoker, D. Qin, G.-K. Plattner, M. Tignor, S. K. Allen, J. Boschung, A. Nauels, Y. Xia, V. Bex, & P. M. Midgley (Eds.), *Climate change 2013: The physical science basis. Contribution of working group i to the fifth assessment report of the intergovernmental panel on climate change* (pp. 659-740). Cambridge, UK and New York, USA: Cambridge University Press.

Neale, R. B., Richter, J. H., Conley, A. J., Park, S., Lauritzen, P. H., Gettelman, A., et al. (2010). *Description of the ncar community
450 atmosphere model (cam 4.0).* Retrieved from Boulder, CO, USA: https://www.ccsm.ucar.edu/models/ccsm4.0/cam/docs/description/cam4_desc.pdf

Otto-Bliesner, B. L., Brady, E. C., Fasullo, J., Jahn, A., Landrum, L., Stevenson, S., et al. (2016). Climate variability and change since 850 ce: An ensemble approach with the community earth system model. *Bulletin of the American Meteorological Society, 97*(5), 735-754. doi:10.1175/BAMS-D-14-00233.1

455 Paaijmans, K. P., Blanford, S., Bell, A. S., Blanford, J. I., Read, A. F., & Thomas, M. B. (2010). Influence of climate on malaria transmission depends on daily temperature variation. *Proceedings of the National Academy of Sciences, 107*(34), 15135. doi:10.1073/pnas.1006422107

Philipona, R., Behrens, K., & Ruckstuhl, C. (2009). How declining aerosols and rising greenhouse gases forced rapid warming in europe since the 1980s. *Geophysical Research Letters, 36*(2). doi:10.1029/2008GL036350

460 Ramanathan, V., Cess, R. D., Harrison, E. F., Minnis, P., Barkstrom, B. R., Ahmad, E., et al. (1989). Cloud-radiative forcing and climate: Results from the earth radiation budget experiment. *Science, 243*(4887), 57-63. doi:10.1126/science.243.4887.57

Robine, J.-M., Cheung, S. L. K., Le Roy, S., Van Oyen, H., Griffiths, C., Michel, J.-P., et al. (2008). Death toll exceeded 70,000 in europe during the summer of 2003. *Comptes Rendus Biologies, 331*(2), 171-178. doi:10.1016/j.crvi.2007.12.001

Rowell, D. P., & Jones, R. G. (2006). Causes and uncertainty of future summer drying over europe. *Climate Dynamics, 27*(2), 281-299.
465 doi:10.1007/s00382-006-0125-9

Ruckstuhl, C., Philipona, R., Behrens, K., Collaud Coen, M., Dürr, B., Heimo, A., et al. (2008). Aerosol and cloud effects on solar brightening and the recent rapid warming. *Geophysical Research Letters, 35*(12). doi:10.1029/2008GL034228

Samset, B., Myhre, G., Forster, P., Hodnebrog, Ø., Andrews, T., Faluvegi, G., et al. (2016). Fast and slow precipitation responses to individual climate forcers: A pdrmip multimodel study. *Geophysical Research Letters, 43*(6), 2782-2791.
470 doi:10.1002/2016GL068064

Samset, B. H., & Myhre, G. (2015). Climate response to externally mixed black carbon as a function of altitude. *Journal of Geophysical Research: Atmospheres, 120*(7), 2913-2927. doi:10.1002/2014JD022849

Schär, C., Vidale, P. L., Lüthi, D., Frei, C., Häberli, C., Liniger, M. A., et al. (2004). The role of increasing temperature variability in european summer heatwaves. *Nature, 427*(6972), 332-336. doi:10.1038/nature02300

475 Schmidt, G. A., Kelley, M., Nazarenko, L., Ruedy, R., Russell, G. L., Aleinov, I., et al. (2014). Configuration and assessment of the giss modele2 contributions to the cmip5 archive. *Journal of Advances in Modeling Earth Systems, 6*(1), 141-184. doi:10.1002/2013MS000265

Seidel, D. J., Fu, Q., Randel, W. J., & Reichler, T. J. (2008). Widening of the tropical belt in a changing climate. *Nature Geoscience, 1*(1), 21-24. doi:10.1038/ngeo.2007.38

480 Seneviratne, S. I., Donat, M. G., Mueller, B., & Alexander, L. V. (2014). No pause in the increase of hot temperature extremes. *Nature Climate Change, 4*, 161. doi:10.1038/nclimate2145

Seneviratne, S. I., Luthi, D., Litschi, M., & Schar, C. (2006). Land-atmosphere coupling and climate change in europe. *Nature, 443*(7108), 205-209. doi:10.1038/nature05095

Shindell, D., & Faluvegi, G. (2009). Climate response to regional radiative forcing during the twentieth century. *Nature Geoscience, 2*(4),
485 294-300. doi:10.1038/Ngeo473

Sillmann, J., Pozzoli, L., Vignati, E., Kloster, S., & Feichter, J. (2013). Aerosol effect on climate extremes in europe under different future scenarios. *Geophysical Research Letters, 40*(10), 2290-2295. doi:10.1002/grl.50459

Smith, S. J., van Aardenne, J., Klimont, Z., Andres, R. J., Volke, A., & Delgado Arias, S. (2011). Anthropogenic sulfur dioxide emissions: 1850–2005. *Atmos. Chem. Phys., 11*(3), 1101-1116. doi:10.5194/acp-11-1101-2011

490 Stjern, C. W., Samset, B. H., Myhre, G., Forster, P. M., Hodnebrog, O., Andrews, T., et al. (2017). Rapid adjustments cause weak surface temperature response to increased black carbon concentrations. *Journal of Geophysical Research-Atmospheres, 122*(21), 11462-11481. doi:10.1002/2017jd027326

Takemura, T., Egashira, M., Matsuzawa, K., Ichijo, H., O'ishi, R., & Abe-Ouchi, A. (2009). A simulation of the global distribution and radiative forcing of soil dust aerosols at the last glacial maximum. *Atmospheric Chemistry & Physics, 9*(9). doi:10.5194/acp-9-
495 3061-2009

Takemura, T., Nozawa, T., Emori, S., Nakajima, T. Y., & Nakajima, T. (2005). Simulation of climate response to aerosol direct and indirect effects with aerosol transport-radiation model. *Journal of Geophysical Research: Atmospheres, 110*(D2). doi:10.1029/2004JD005029

Tang, Q., & Leng, G. (2012). Damped summer warming accompanied with cloud cover increase over eurasia from 1982 to 2009. *Environmental Research Letters, 7*(1), 014004. doi:10.1088/1748-9326/7/1/014004

Tang, T., Shindell, D., Faluvegi, G., Myhre, G., Olivié, D., Voulgarakis, A., et al. (2019). Comparison of effective radiative forcing calculations using multiple methods, drivers, and models. *Journal of Geophysical Research: Atmospheres, 124*(8), 4382-4394. doi:10.1029/2018JD030188

Tang, T., Shindell, D., Samset, B. H., Boucher, O., Forster, P. M., Hodnebrog, Ø., et al. (2018). Dynamical response of mediterranean precipitation to greenhouse gases and aerosols. *Atmospheric Chemistry and Physics, 18*(11), 8439-8452. doi:10.5194/acp-18-8439-2018

Turner, A. G., & Annamalai, H. (2012). Climate change and the south asian summer monsoon. *Nature Climate Change, 2*(8), 587-595. doi:10.1038/nclimate1495

Vasseur David, A., DeLong John, P., Gilbert, B., Greig Hamish, S., Harley Christopher, D. G., McCann Kevin, S., et al. (2014). Increased temperature variation poses a greater risk to species than climate warming. *Proceedings of the Royal Society B: Biological Sciences, 281*(1779), 20132612. doi:10.1098/rspb.2013.2612

Vautard, R., Yiou, P., D'Andrea, F., de Noblet, N., Viovy, N., Cassou, C., et al. (2007). Summertime european heat and drought waves induced by wintertime mediterranean rainfall deficit. *Geophysical Research Letters, 34*(7). doi:10.1029/2006GL028001

Walters, D., Williams, K., Boutle, I., Bushell, A., Edwards, J., Field, P., et al. (2014). The met office unified model global atmosphere 4.0 and jules global land 4.0 configurations. *Geoscientific Model Development, 7*(1), 361-386. doi:10.5194/gmd-7-361-2014

Wang, C. (2007). Impact of direct radiative forcing of black carbon aerosols on tropical convective precipitation. *Geophysical Research Letters, 34*(5). doi:10.1029/2006GL028416

Wang, G., & Dillon, M. E. (2014). Recent geographic convergence in diurnal and annual temperature cycling flattens global thermal profiles. *Nature Climate Change, 4*(11), 988-992. doi:10.1038/Nclimate2378

Watanabe, M., Suzuki, T., O'ishi, R., Komuro, Y., Watanabe, S., Emori, S., et al. (2010). Improved climate simulation by miroc5: Mean states, variability, and climate sensitivity. *Journal of Climate, 23*(23), 6312-6335. doi:10.1175/2010JCLI3679.1

Wetherald, R. T., & Manabe, S. (1995). The mechanisms of summer dryness induced by greenhouse warming. *Journal of Climate, 8*(12), 3096-3108. doi:10.1175/1520-0442(1995)008<3096:TMOSDI>2.0.CO;2

Wild, M., Ohmura, A., Gilgen, H., & Rosenfeld, D. (2004). On the consistency of trends in radiation and temperature records and implications for the global hydrological cycle. *Geophysical Research Letters, 31*(11). doi:10.1029/2003GL019188

Williams, K. D., Jones, A., Roberts, D. L., Senior, C. A., & Woodage, M. J. (2001). The response of the climate system to the indirect effects of anthropogenic sulfate aerosol. *Climate Dynamics, 17*(11), 845-856. doi:10.1007/s003820100150

Wood, R., & Bretherton, C. S. (2006). On the relationship between stratiform low cloud cover and lower-tropospheric stability. *Journal of Climate, 19*(24), 6425-6432. doi:10.1175/JCLI3988.1

Xu, Y. Y., Lamarque, J. F., & Sanderson, B. M. (2018). The importance of aerosol scenarios in projections of future heat extremes. *Climatic Change, 146*(3-4), 393-406. doi:10.1007/s10584-015-1565-1

Zampieri, M., D'Andrea, F., Vautard, R., Ciais, P., de Noblet-Ducoudré, N., & Yiou, P. (2009). Hot european summers and the role of soil moisture in the propagation of mediterranean drought. *Journal of Climate, 22*(18), 4747-4758. doi:10.1175/2009JCLI2568.1

Zelinka, M. D., Randall, D. A., Webb, M. J., & Klein, S. A. (2017). Clearing clouds of uncertainty. *Nature Climate Change, 7*(10), 674-678. doi:10.1038/nclimate3402

Zhai, C. X., Jiang, J. H., & Su, H. (2015). Long-term cloud change imprinted in seasonal cloud variation: More evidence of high climate sensitivity. *Geophysical Research Letters, 42*(20), 8729-8737. doi:10.1002/2015gl065911

Zhou, C., Zelinka, M. D., & Klein, S. A. (2016). Impact of decadal cloud variations on the earth's energy budget. *Nature Geoscience, 9*, 871. doi:10.1038/ngeo2828

550 **Table 1.** Descriptions of the nine PDRMIP models used in this study, adapted from Tang et al. (2019).

Model name	Version	Resolution	Ocean setup	Aerosol setup	references
CanESM	2010	2.8×2.8 35 levels	Coupled	Emission	Arora et al. (2011)
GISS-E2	E2-R	2×2.5 40 levels	Coupled	Fixed concentration	Schmidt et al. (2014)
HadGEM2-ES	6.6.3	1.875×1.25 38 levels	Coupled	Emissions	Collins et al. (2011)
HadGEM3	GA 4.0	1.875×1.25 85 levels	Coupled	Fixed concentration	Bellouin et al. (2011) Walters et al. (2014)
MIROC-SPRINTARS	5.9.0	T85 40 levels	Coupled	HTAP2 emissions	Takemura et al. (2009) Takemura et al. (2005) Watanabe et al. (2010)
CESM-CAM4	1.0.3	2.5×1.9 26 levels	Slab	Fixed concentration	Neale et al. (2010) Gent et al. (2011)
CESM-CAM5	1.1.2	2.5×1.9 30 levels	Coupled	Emissions	Hurrell et al. (2013) Kay et al. (2015) Otto-Bliesner et al. (2016)
NorESM	1-M	2.5×1.9 26 levels	Coupled	Fixed concentration	Bentsen et al. (2013) Iversen et al. (2013) Kirkevåg et al. (2013)
IPSL-CM	5A	3.75×1.9 19 levels	Coupled	Fixed concentration	Dufresne et al. (2013)

Note: GA = Global Atmosphere. HTAP2 = Hemispheric Transport Air Pollution, Phase 2.

555

560

Table 2. Domain-averaged Tmax changes from each radiative component estimated from the linear models (unit: K).

$CO_2 \times 2$				
Region	$SW_{clear-sky}$	SWCRE	↓LW	Total
N. America	-0.27 ± 0.01	0.95 ± 0.02	3.24 ± 0.03	3.92 ± 0.06
Europe	-0.24 ± 0.01	1.14 ± 0.03	2.79 ± 0.02	3.69 ± 0.06
E. China	-0.23 ± 0.01	0.71 ± 0.02	2.82 ± 0.02	3.30 ± 0.05
India	-0.29 ± 0.01	0.26 ± 0.01	2.59 ± 0.02	2.56 ± 0.04
$BC \times 10$				
Region	$SW_{clear-sky}$	SWCRE	↓LW	Total
N. America	-0.56 ± 0.03	1.00 ± 0.02	1.94 ± 0.04	2.38 ± 0.10
Europe	-0.73 ± 0.04	1.15 ± 0.03	1.32 ± 0.03	1.74 ± 0.10
E. China	-1.40 ± 0.08	0.98 ± 0.02	1.92 ± 0.04	1.50 ± 0.15
India	-0.89 ± 0.05	-1.05 ± 0.02	1.10 ± 0.02	-0.84 ± 0.05

565 Note: uncertainty range was estimated from the 95% confidence interval of each coefficient.

570

575
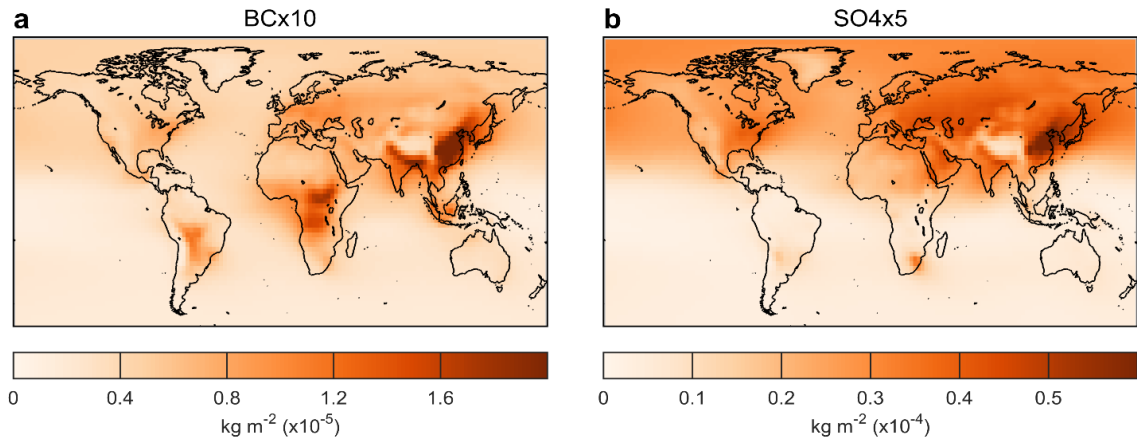
580 **Figure 1: Aerosol loadings for the two aerosol experiments in CanESM2 model (as an illustrative example).**

585

590
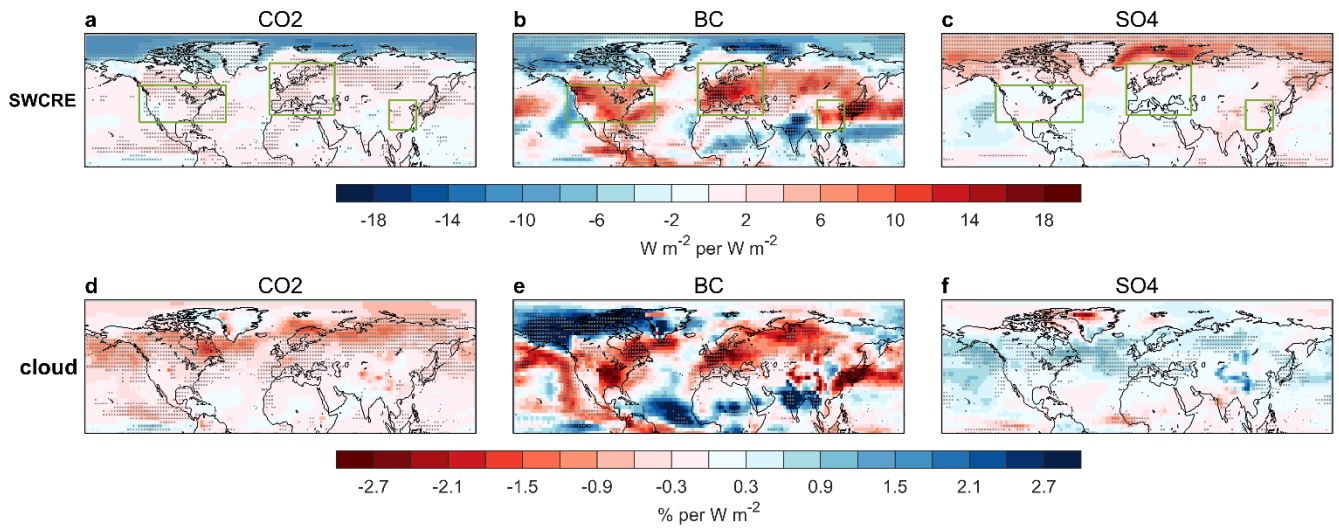
Figure 2: SWCRE changes (a-c) and cloud cover changes per unit forcing at 850 hPa (d-f) in JJA, results for SO4 are changes per negative forcing. Grey dots indicate changes are significant at 0.05 level. Positive anomalies in a-c indicate more radiation reaching the surface.

595

600
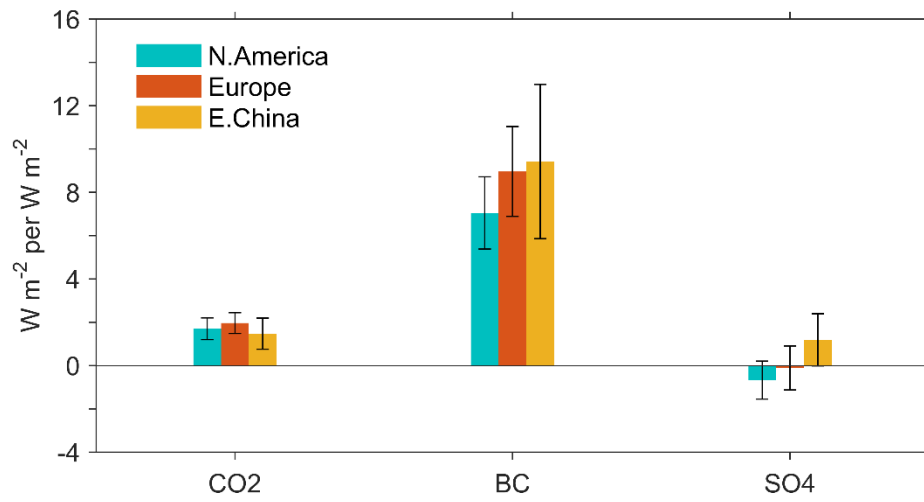
605

Figure 3: Domain-averaged SWCRE changes for three regions (green boxes in Fig. 2). Bars represent MMM results and errorbars indicate one standard error across the models.

610

615
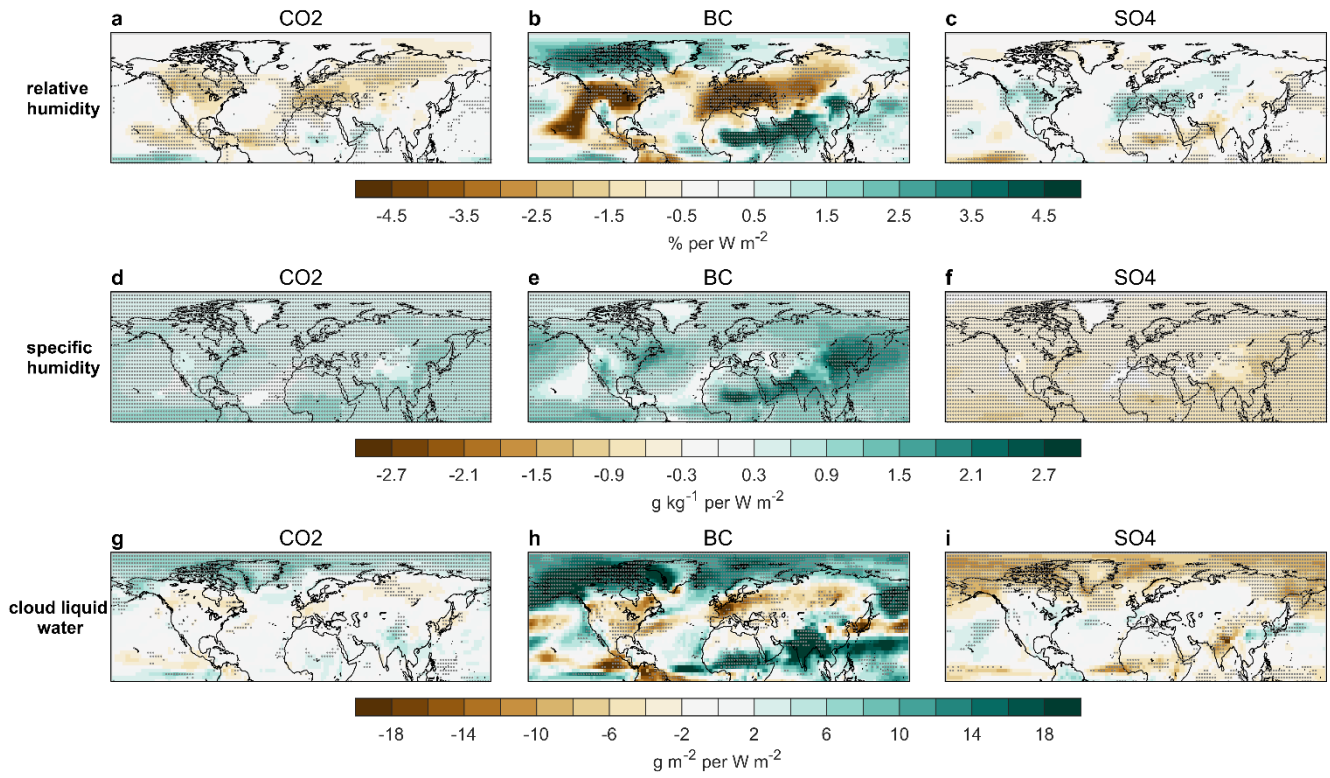
Figure 4: Same as Figure 2, but for humidity at 850 hPa.

620

625
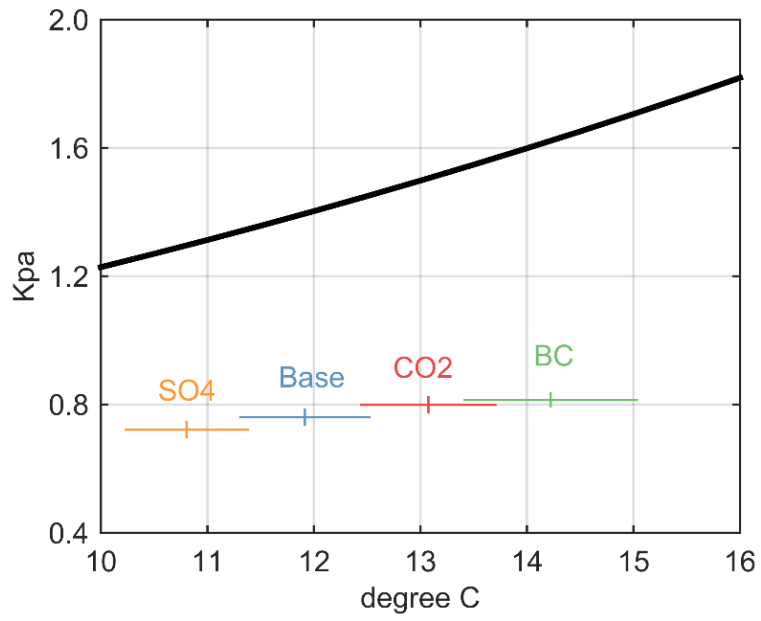
Figure 5: Domain-averaged vapor pressure changes per unit forcing as a function of temperature at 850 hPa for Europe. Errorbars indicate one standard error across the models. The thick black line represents saturation vapor pressure.

630

635

640

645
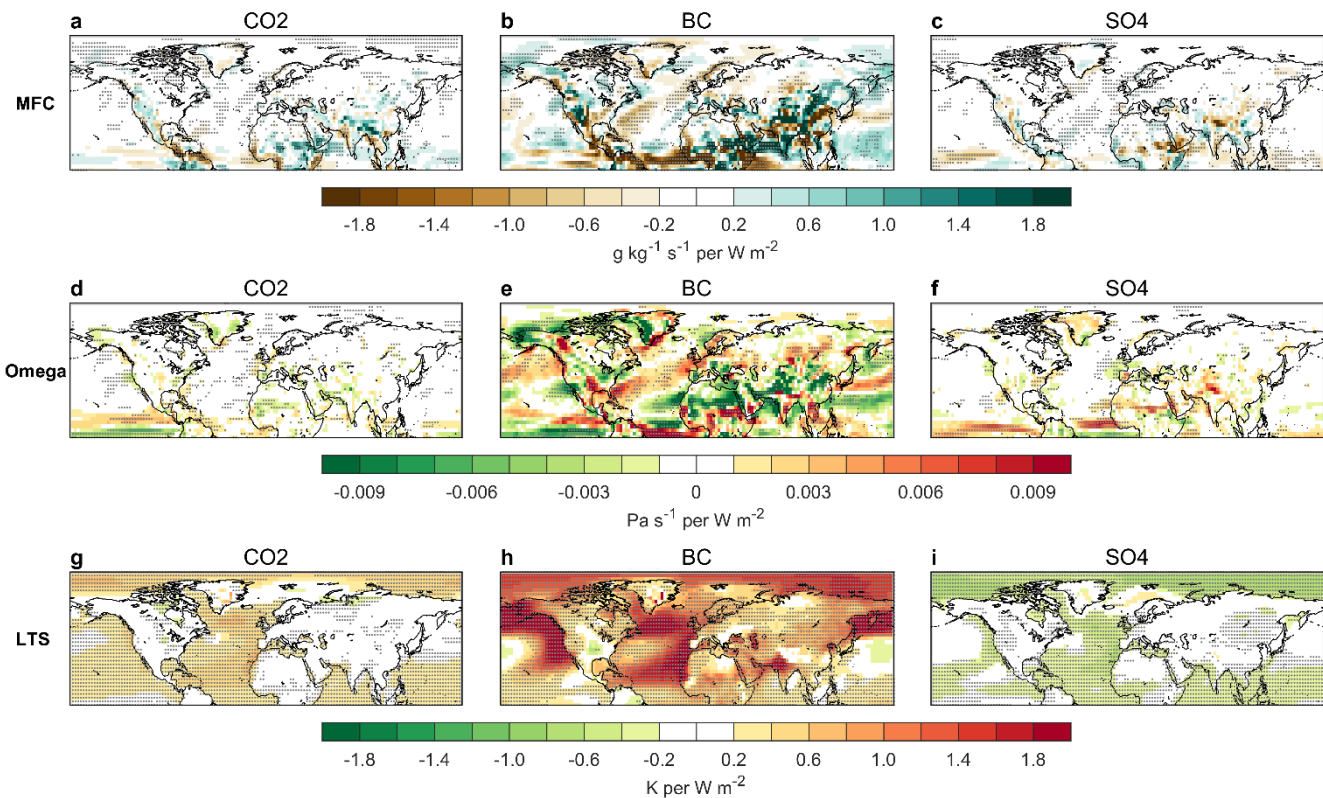
Figure 6: Same as Fig. 2, but for changes of moisture flux convergence (MFC, a-c), vertical velocity (omega, d-f) and lower tropospheric stability (LTS, g-i) per unit forcing. For vertical velocity (omega), positive anomalies indicate the air is less convective. LTS is calculated as the difference of potential temperature between 700 hPa and the surface. Positive LTS anomalies in g-i indicate stronger inversion or weaker lapse rate.
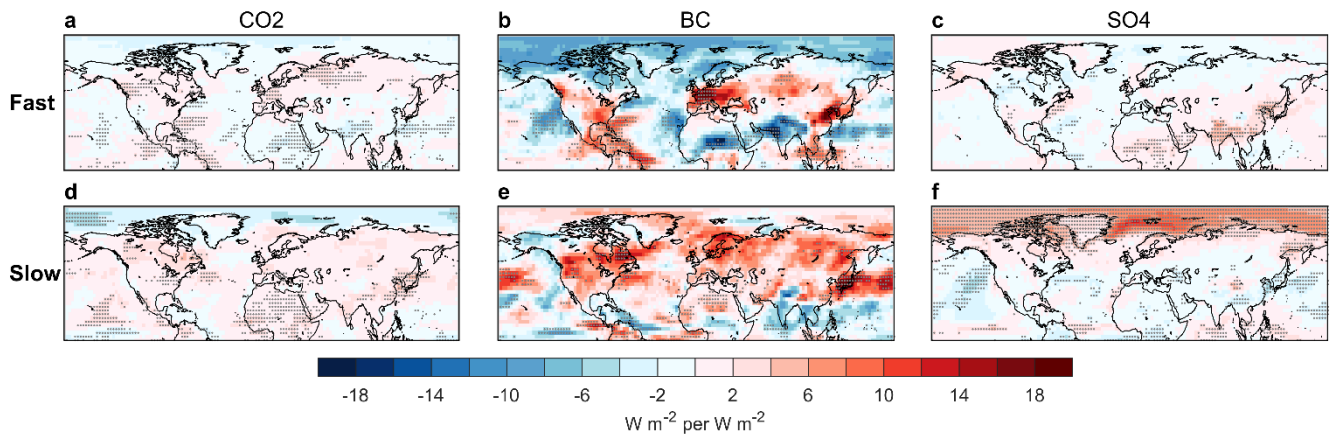
Figure 7: Same as Figure 2 (d-f), but for fast (a-c) and slow responses (d-f) of SWCRE changes per unit forcing.

670

675

680

685
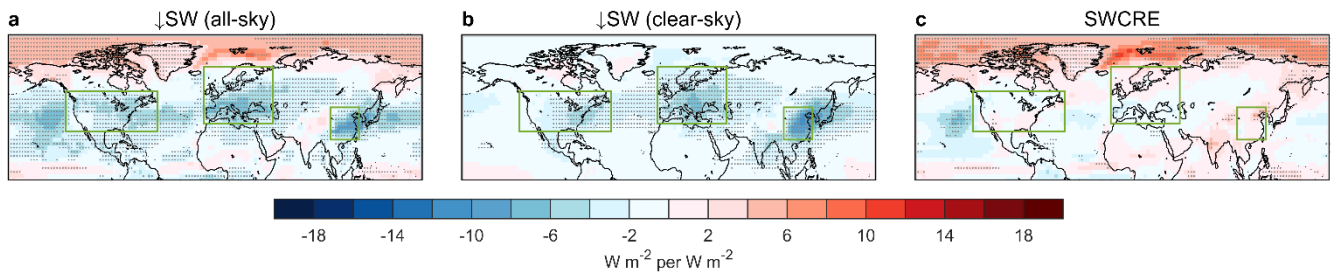
Figure 8: Changes of SW flux per unit negative forcing under all-sky (a), clear-sky (b) conditions and their difference (c) for the SO₄ experiment.

690

695

700
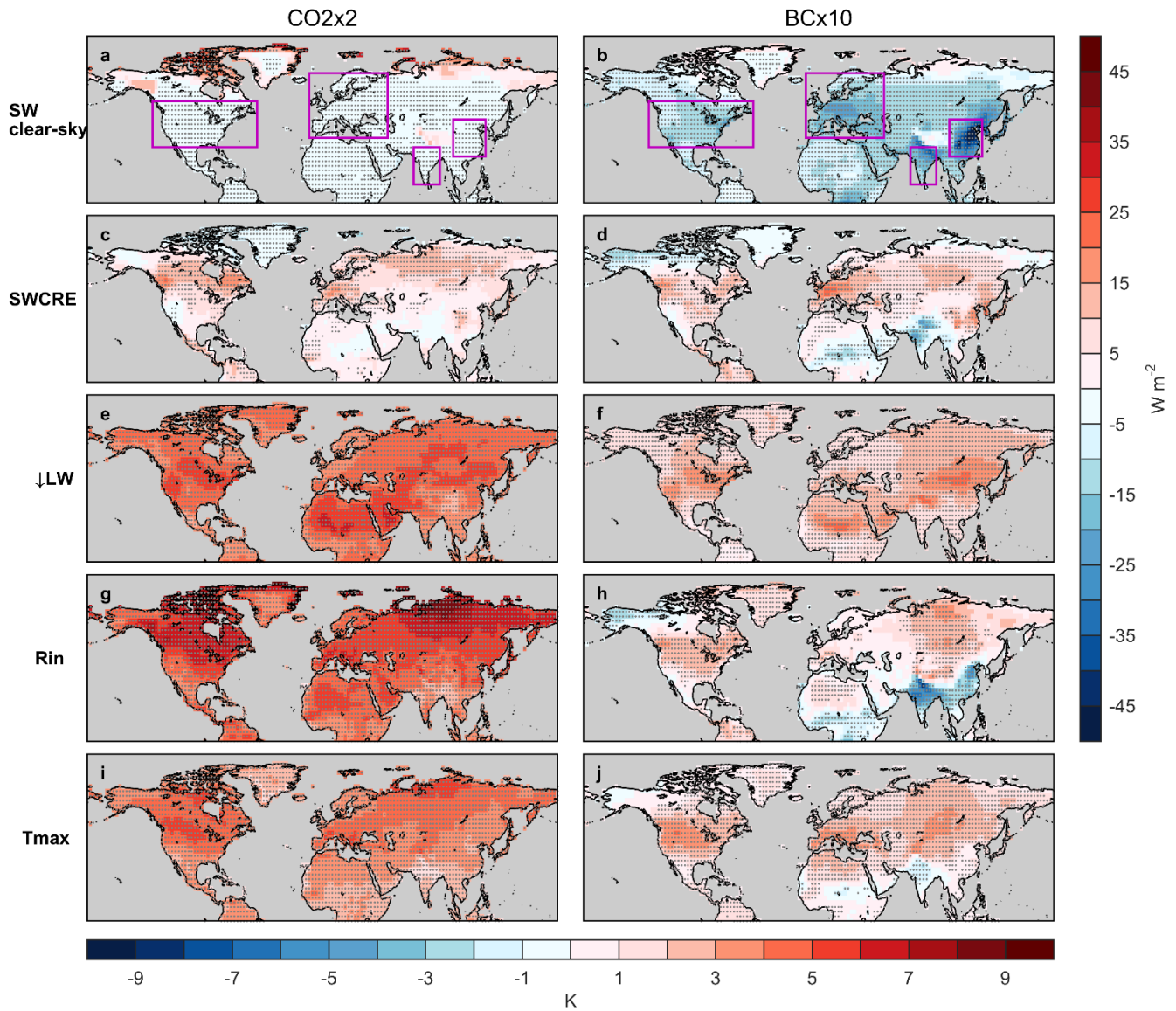
Figure 9: Changes of Rin and its components (a-h) as well as changes of Tmax (i-j) for the CO$_2$×2 (left) and BC×10 (right) experiments (original output, no normalization applied).

705
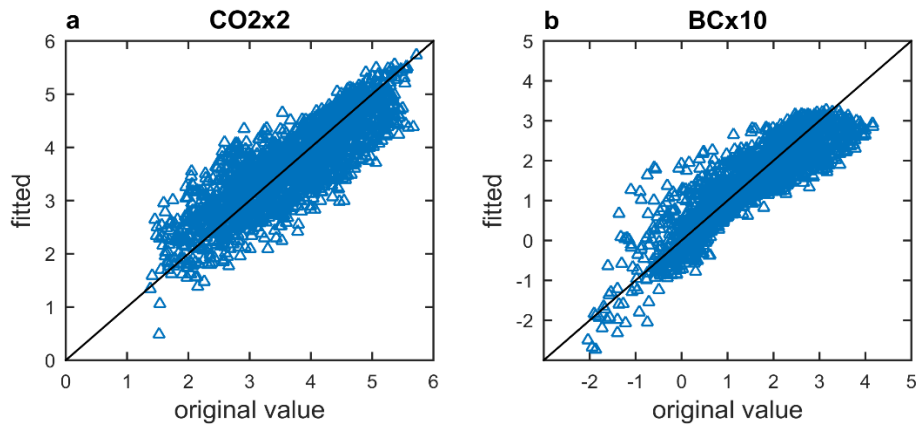
Figure 10: Comparison of fitted Tmax from the linear models vs original Tmax values. Blue triangles are values for all grid boxes over NH and black solid line represents one-one line.

710

715

720

725
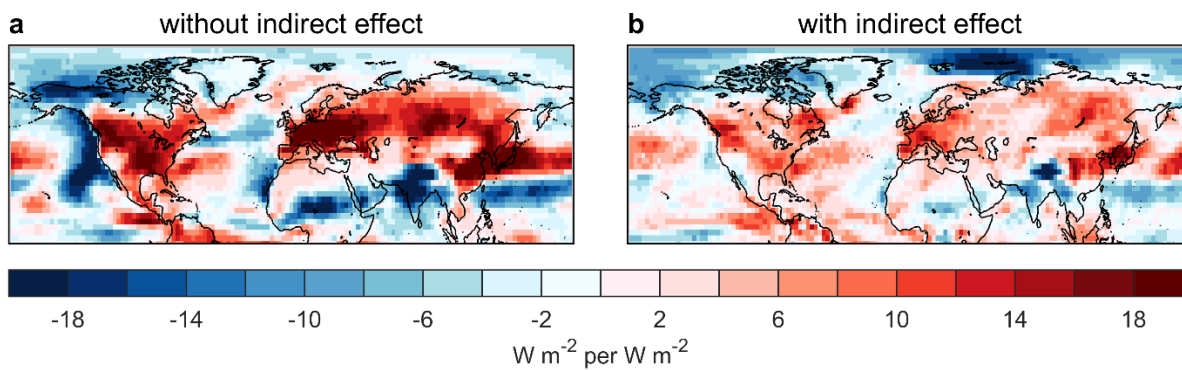
Figure 11: SWCRE changes for the BC experiment, (a) for models without aerosol indirect effects and (b) for models with indirect effects.